
Copyright 2018, ABRACO

Trabalho apresentado durante o INTERCORR 2018, em São Paulo, no mês de maio de 2018.

As informações e opiniões contidas neste trabalho são de exclusiva responsabilidade do(s) autor(es).

Effect of post weld heat treatment on corrosion resistance of austenitic stainless steel weldment joint by nickel filler metal

^aJoão Henrique Nery Garcia , ^aThaís Rachid Netto , ^bLuiza Esteves , ^cWagner Reis da Costa Campos , ^cEmerson Giovani Rabelo

Abstract

Dissimilar metal welds between austenitic stainless steel and nickel alloys may require post-weld heat treatment (PWHT) to relieve stresses from the welding process. The PWHT and welding process results in microstructural variations in materials that can affect their mechanical properties and corrosion resistance. The influence of different PWHT on corrosion behavior of a dissimilar weld joint of AISI 316L plates and nickel alloy as filler material in saline environments was evaluated. The material was submitted to heat treatments for three hours at 600, 700 and 800 °C. Cyclic potentiodynamic polarization (CPP) and electrochemical impedance spectroscopy (EIS) were used to evaluate the corrosion behavior of samples of weld joints and base metal (BM), before and after PWHT, in acidified sodium chloride solutions. A similar corrosion resistance was observed to base metal for all PWHT using EIS experiments. CPP curves for the weld joints demonstrated an increase of pitting corrosion resistance as the PWHT temperature increases, due to a decrease of delta ferrite.

Keywords: 316L, Alloy 182, Cyclic potentiodynamic polarization, Dissimilar weld joints, Electrochemical impedance spectroscopy

Introduction

Austenitic stainless steel and nickel base alloys are generally employed in plants of energy generations, nuclear power plants, chemical and petrochemical industries, due to their high corrosion resistance (1–6). Nickel base alloys are frequently used as filler metal in dissimilar metal welds between ferritic and stainless steel base metals (7). The structural integrity of these welds is a key factor for a safe and continuous operation of these plants (8).

During welding process of austenitic stainless steel, residual stresses can be induced due to the low thermal conductivity and high coefficient of expansion of austenitic stainless steel (9–11). In order to relief the residual stress, post weld heat treatments (PWHT) are generally applied to austenitic materials in temperature range from 480 to 925 °C. However, it may result in sensitizing susceptible materials and should only be used for low carbon grades and stabilized steels (4), (7), (10–12).

^a Engenheiro Químico-Estudante de Mestrado - CENTRO DE DESENVOLVIMENTO DA TECNOLOGIA NUCLEAR

^b Doutorado -Pós doc - CENTRO DE DESENVOLVIMENTO DA TECNOLOGIA NUCLEAR

^c Doutorado-Pesquisador - CENTRO DE DESENVOLVIMENTO DA TECNOLOGIA NUCLEAR

Mechanical properties and corrosion resistance of the weld metals depends on the change of the microstructure during welding process and PWHT. The thermal cycle that occurs during welding affects the microstructure and surface composition of welds. Hence, the corrosion resistance of weld may be inferior to the resistance of base metal (BM), due to precipitation, microsegregation, the formation of unmixed zones, contamination of the solidifying weld pool, secondary phase and recrystallization and grain growth in the weld heat-affected zone (HAZ) (13), (14).

Despite its beneficial effect in reducing crack susceptibility, the presence of delta ferrite can be detrimental to the corrosion resistance of austenitic stainless steel (3), (15). The solubilization of delta ferrite occurs as temperature increases above 500 °C. During its solubilization, ferrite is transformed into austenite, carbides and second phases. The main intermetallic phase in AISI 316L is sigma phase (9), (16), (17). This phase is hard and brittle causing deterioration of mechanical properties and promotes Cr and Mo depletion near the precipitates, decreasing the corrosion resistance of the steel (18–22).

The influence of PWHT at different temperatures on corrosion behavior of a weld joint between AISI 316L stainless steel plates and nickel-base alloy 182 as filler material in sodium chloride solution was investigated in this work using cyclic potentiodynamic polarization and electrochemical impedance spectroscopy (EIS).

Materials and Methods

Two plates of stainless steel AISI 316L with 300 mm (length), 150 mm (width), and 12.7 mm (thickness) were welded by shielded metal arc welding (SMAW). The filler metal was nickel-base alloy 182 with diameters of 2.5 mm and 3.2 mm. The nominal chemical composition of the base and the filler metal are shown in Table 1. For the welding process, the plates of stainless steel AISI 316L were prepared employing a single V groove edge preparation with an included angle of 30°. The top plates were welded with a narrow gap of 2.5 mm in seven passes with pre-heating at 150 °C, and interpass temperature between 100 °C to 150 °C. The weld root was performed with (90-100) A with filler metal of 2.5 mm. The other beads were performed with (110-120) A and filler metal of 3.2 mm. After welding, the weld joint was submitted to heat treatments for three hours at 600, 700 and 800 °C to relieve stresses of the welded joints.

The welded samples were cut transversely to the welding direction. The sample location was the weld root. The specimens were mechanically polished with 1 µm and electrolytically etched in a 10% oxalic acid solution at 2.2 V DC for 60 s in order to examine the microstructure, to identify grains, dendrite boundaries, and precipitates in base metal (BM), weld joint and weld metal. The microstructures analyses were carried out by an optical microscope.

The specimens for electrochemical measurements were weld to a copper wire for electrical contact, and embedded in epoxy resin. The working surface was then abraded with SiC papers of grit size from 80 to 600 mesh and cleaned with distilled water and alcohol. The surface area of the samples was measured by Image J software. The average size of areas was about 2.0 cm².

Electrochemical measurements were performed using an Autolab PGSTAT 20 potentiostat and an electrochemical cell of three electrodes: BM and the welded samples as working electrode, platinum mesh as counter electrode and silver chloride electrode (Ag/AgCl, 3M KCl) as reference electrode. The electrochemical tests were carried out at 25 °C in a solution containing 190 g/L NaCl, 0.4 g/L sodium acetate and pH 4.0.

The open circuit potential (OCP) was recorded for 1 h or until stabilization, and the CPP curves were collected by scanning to the anodic direction at a scan rate of 0.167 mV/s, -0.02 V(Ag/AgCl, 3M KCl) from the stabilized OCP. When the current reached 1 mA/cm² the scan was reversed. All the electrochemical measurements were repeated at least three times to ensure the reproducibility. The pitting potential (E_{pit}) was defined as the potential value at which the current density sharply rose. After the CPP tests, surface morphology was examined using an optical microscope and scanning electron microscope (SEM).

Electrochemical impedance spectroscopy (EIS) was performed after monitoring the OCP for 1 h or until to obtain a stable open circuit potential value. The amplitude sine-wave of the applied potential is 10 mV from 10 kHz to 10 mHz with 10 points per decade. The measurements were performed in triplicate to ensure the reproducibility. The experimental impedance spectra were fitted using Z-View software version 3.4d.

Results and discussion

The AISI 316L microstructure consists of austenite grains and stringers of delta ferrite. The increase of PWHT temperature causes the solubilization of delta ferrite as shown in Figure 1. The delta ferrite content was measured for the BM by image analyzing software for microstructure analyzing Quantikov, and shown in Table 2 (23). Close to the fusion line, the delta ferrite, which was partially dissolved by welding process, also decreased with an increasing temperature of PWHT. The delta ferrite content of the base and weld metals decreased with an increase in the annealing temperature (24), (25). The microstructure of weld metal consists of dendrite grains, with inclusions and precipitates. The amount of precipitates in the weld metal decreased with an increase in temperature of the PWHT.

Figure 2 shows the CPP curves for BM and weld joints, before and after PWHT, in a 190 g/L NaCl + 0.4 g/L sodium acetate solution (pH 4.0). It is known that acidic environments containing chloride leads to severe pitting corrosion. The electrochemical parameters from CPP curves, such as corrosion potential (E_{corr}), passive current (I_{pass}), pitting potential (E_{pit}) and protection potential (E_{prot}), are shown in Table 3.

The CPP curves showed that PWHT has no influence on E_{corr} value. E_{corr} was measured around -200 mV (Ag/AgCl 3M KCl) for all specimens. Although all specimens showed a passive behavior, the weld joint of PWHT 800 °C showed a wider and more defined passive region. The increasing of PWHT temperature led to an increase of E_{pit} and a decrease of E_{prot} . The increase of E_{pit} could be related with a higher solubilization of delta ferrite at higher temperatures. Delta ferrite provides favorable sites for pitting initiation, resulting in deleterious effects on corrosion resistance (26–30). The weld joint heat treated at 600 °C has similar corrosion behavior compared to the as-welded joint. The BM showed better corrosion

resistance than the weld joint (31–33). E_{pit} clearly shift towards higher values and the passive region becomes wider for BM.

After CPP, the specimens were observed in MEV for metallographic examination (Figure 3). It revealed pitting attack near the fusion line in the weld metal, since the local properties of the fusion zone are often inferior to those of the BM, which can be attributed to segregation during solidification. The pit diameter depends on PWHT temperature and its morphology are roughly circular or elliptical. Larger pits were encountered at higher PWHT temperature. At higher PWHT temperature, the hysteresis loop ($E_{\text{pit}} - E_{\text{prot}}$) was larger, showing a difficulty of the sample to attain the passive layer. It is known that the pit grows between E_{pit} and E_{prot} , after its initiation (34), (35).

Nyquist diagrams of BM before and after PWHT are shown in Figure 4. The EIS data were fitted with two-time constants as an equivalent electrochemical circuit shown in Figure 4. In Figure 4 where, R_s is the solution resistance and, R_{pore} is the porous resistance resulted from the formation of ionically conducting paths across the passive layer. CPE_1 represents the constant phase element of the passive film formed, coupled with a resistance due to the ionic paths through the oxide film. CPE_2 represents the constant phase element at the interfaces and R_{ct} represents the corresponding charge-transfer (R_{ct}) resistance. A pure capacitor was used if $n=1$ and a constant phase element (CPE) was used if $0 < n < 1$, due to the non-ideal capacitive response. The average of polarization resistance (R_p) between the measurements in each solution is shown in Figure 5. The BM as welded had a similar corrosion behavior compared to the BM treated at 600 °C, 700 °C. The BM treated at 800 °C showed a slight better corrosion resistance than the previous one

Conclusion

The higher solubilization of delta ferrite and the decrease of microsegregation at higher PWHT temperatures led to an increase of corrosion resistance. The sample heat treated at 800 °C had a wider and more defined passive region and the highest pitting potential, providing a better corrosion resistance to the weld joint. On the other hand, this sample showed the lowest protection potential and, consequently a higher hysteresis loop, resulting in larger pits. The corrosion resistance of the sample after PWHT at 600 °C was similar to the as-welded sample. The corrosion resistance of the weld joints was lower than the Bm before and after PWHT.

References

- (1) NELSON, T.W. ; LIPPOLD, J.C. ; MILLS, M.J.: Nature and Evolution of the Fusion Boundary in Ferritic-Austenitic Dissimilar Metal Welds — Part 1 : Nucleation and Growth. **Welding Journal**, p. 329s–337s, 2009.
- (2) NELSON, T.W. ; LIPPOLD, J.C. ; MILLS, M.J.: Nature and Evolution of the Fusion Boundary in Ferritic-Austenitic Dissimilar Metal Welds — Part 2: On-Cooling Transformations. **Welding Journal**, p. 267s–277s, 2010.
- (3) GILL, T. P. S. et al. On microstructure-property correlation of thermally aged type 316L stainless steel weld metal. **Metallurgical Transactions A**, v. 20, n. 6, p. 1115–1124, 1989.

- (4) ROWE, M. D.; NELSON, T. W.; LIPPOLD, J. C. Hydrogen-Induced Cracking along the fusion boundary of dissimilar metal welds. **Welding Research Supplement**, p. 31–37, 1999
- (5) GUPTA, K.; CHHIBBER, R. Structural integrity of bimetallic welds at elevated temperature. **International Journal of Mechanical Engineering and Technology (Ijmet)**, v. 3, n. 1, p. 235–243, 2012.
- (6) SARIKKA, T. et al. Microstructural, mechanical, and fracture mechanical characterization of SA 508-Alloy 182 dissimilar metal weld in view of mismatch state. **International Journal of Pressure Vessels and Piping**, v. 145, n. October, p. 13–22, 2016
- (7) MITEVA, R.; TAYLOR, N. G. **General Review of Dissimilar Metal Welds in Piping Systems of Pressurised Water Reactors, Including WWER Designs**. Petten: European Commission, 2006
- (8) SCHVARTZMAN, M. M. DE A. M. et al. Avaliação da suscetibilidade à corrosão sob tensão da ZAC do aço inoxidável AISI 316L em ambiente de reator nuclear PWR. **Soldagem e Inspeção**, v. 14, n. 3, p. 228–237, 2009.
- (9) LO, I. H.; TSAI, W. T. Effect of heat treatment on the precipitation and pitting corrosion behavior of 347 SS weld overlay. **Materials Science and Engineering A**, v. 355, n. 1–2, p. 137–143, 2003.
- (10) SMITH, J.; FARRAR, R. Influence of microstructure and composition on mechanical properties of some AISI 300 series weld metals. **International materials reviews**, v. 38, n. 1, p. 3–9, 1993.
- (11) TSAI, W. T.; YU, C. L.; LEE, J. I. Effect of heat treatment on the sensitization of Alloy 182 weld. **Scripta Materialia**, v. 53, n. 5, p. 505–509, 2005.
- (12) SIREESHA, M.; ALBERT, S. K.; SUNDARESAN, S. Metallurgical changes and mechanical behaviour during high temperature aging of welds between Alloy 800 and 316LN austenitic stainless steel. **Materials Science and Technology**, v. 19, n. October, p. 1411–1417, 2003.
- (13) CUI, Y.; LUNDIN, C. D. Austenite-preferential corrosion attack in 316 austenitic stainless steel weld metals. **Materials and Design**, v. 28, n. 1, p. 324–328, 2007.
- (14) LU, B. T. et al. Pitting and stress corrosion cracking behavior in welded austenitic stainless steel. **Electrochimica Acta**, v. 50, n. 6, p. 1391–1403, 2005.
- (15) PUJAR, M. G. et al. Evaluation of Microstructure and Electrochemical Corrosion Behavior of Austenitic 316 Stainless Steel Weld Metals with Varying Chemical Compositions. **Journal of Materials Engineering and Performance**, v. 14, n. 3, p. 327–342, 2005.
- (16) KOŽUH, S.; GOJIĆ, M.; KOSEC, L. The effect of annealing on properties of AISI 316L base and weld metals. **Materials and Geoenvironment**, v. 54, n. 3, p. 331–344, 2007.
- (17) SCHWIND, M et al. Sigma-Phase Precipitation in Stabilized Austenitic Stainless Steels. **Acta Materialia**. v. 48, n. 10, p. 2473–2481, 2000.
- (18) VILLANUEVA, D. M. E. et al. Comparative study on sigma phase precipitation of three types of stainless steels: austenitic, superferritic and duplex. **Materials Science and Technology**, v. 22, n. 9, p. 1098–1104, 2006.
- (19) TAVARES, S. S. M. et al. Influência dos tratamentos térmicos de estabilização e solubilização na resistência à corrosão intergranular do aço inoxidável Aisi 347 fundido. **Tecnologia em Metalurgia e Materiais** v. 4, n. 3, p. 18–22, 2008.

-
- (20) HSIEH, C. C.; LIN, D. Y. ; WU, W. Precipitation behavior of σ phase in 19Cr–9Ni–2Mn and 18Cr–0.75Si stainless steels hot-rolled at 800 °C with various reduction ratios. **Materials Science and Engineering A**. v. 467, n. 1–2, p. 181–189, 2007.
- (21) MACHADO, I. F. ; PADILHA, A. F. Aging behaviour of 25Cr 17Mn high nitrogen duplex stainless. **Iron & Steel Institute of Japan**. v. 40, n. p. 719-724. 2000.
- (22) NORSTRÖM, L. ; PETTERSSON, S. ; NORDIN, S. σ Phase Embrittlement in Some ferritic-austenitic stainless steels. **Materialwissenschaft und Werkstofftechnik** v. 12, n. 7, p. 229–234, 1981.
- (23) PINTO, L. C. M. **Quantikov: Um analisador microestrutural para o ambiente Windows**. 1996. Tese (Doutorado) 160 f. Instituto de Pesquisas Energéticas e Nucleares. Universidade de São Paulo - USP, São Paulo, 1996
- (24) PADILHA, A. F.; RIOS, P. R. Decomposition of Austenite in Austenitic Stainless Steels. **ISIJ International**, v. 42, n. 4, p. 325–327, 2002.
- (25) KOŽUH, S.; GOJI, M. Mechanical properties and microstructure of austenitic stainless steel after welding and post-weld heat treatment. **Kovove Materijally**, v. 47, p. 253–262, 2009.
- (26) KOZUH, S.; GOJIC, M.; ROKOVIC, M. K. The effect of PWHT on electrochemical behaviour of AISI 316L weld metal. **Chemical and Biochemical Engineering Quarterly**, v. 22, n. 4, p. 421–431, 2008.
- (27) FARID, M.; MOLLIAN, P. A. High-brightness laser welding of thin-sheet 316 stainless steel. **Journal of Materials Science** v. 35, n. 15, p. 3817–3826, 2000.
- (28) ZUMELZU, E.; SEPÚLVEDA, J.; IBARRA, M. Influence of microstructure on the mechanical behaviour of welded 316 L SS joints. **Journal of Materials Processing Technology**, v. 94, n. 1, p. 36–40, 1999.
- (29) CUI, Y.; LUNDIN, C. D. Austenite-preferential corrosion attack in 316 austenitic stainless steel weld metals. **Materials and Design**, v. 28, n. 1, p. 324–328, 2007.
- (30) GILL, T. P. S.; GNANAMOORTHY, J. B.; PADMANABHAN, K. A. Influence of Secondary Phases on the Localized Corrosion of Thermally Aged Aisi 316L Stainless Steel Weld Metal. **Corrosion**, v. 43, n. 4, p. 208–213, 1987
- (31) REDDY, G. M. et al. Influence of welding techniques on microstructure and pitting corrosion behaviour of 1441 grade Al-Li alloy gas tungsten arc welds. **British Corrosion Journal**, v. 36, n. 4, p. 304–309, 2001.
- (32) GARCIA, C. et al. Pitting corrosion of welded joints of austenitic stainless steels studied by using an electrochemical minicell. **Corrosion Science**, v. 50, n. 4, p. 1184–1194, 2008.
- (33) BLASCO-TAMARIT, E. ; IGUAL-MUÑOZ, A. ; GARCÍA ANTÓN, J. ; GARCÍA-GARCÍA, D. Effect of aqueous LiBr solutions on the corrosion resistance and galvanic corrosion of an austenitic stainless steel in its welded and non-welded condition. **Corrosion Science** v. 48, n. 4, p. 863–886, 2006.
- (34) WILDE, B. E. A critical appraisal of some popular laboratory electrochemical tests for predicting the localized corrosion resistance of stainless alloys in sea water. **Corrosion**, v. 28, n. 8, p. 283–291, 1972.
- (35) CHEN, Y. Y.; CHOU, L. B.; SHIH, H. C. Effect of solution pH on the electrochemical polarization and stress corrosion cracking of Alloy 690 in 5 M NaCl at room temperature. **Materials Science and Engineering A**, v. 396, n. 1–2, p. 129–137, 2005.

Tables

Table 1 - Nominal chemical composition of base metal (AISI 316L) and filler metal (alloy 182) (% in weight)

Material	Cu	Co	Cr	Mo	Fe	Si	Mn	C	Ti	S	P	Nb	Ni
AISI 316L	-	-	16.000	2.000	Bal.	0.750	2.000	0.030	-	0.030	0.045	-	10.000
Alloy 182	0.040	0.050	16.533	-	3.580	0.506	5.703	0.026	0.116	0.008	0.010	1.910	Bal.

Table 2 - Delta ferrite content measured by color analyzing software.

Sample	Delta ferrite content (%)
BM No PWHT	3.46 ± 0.63
BM PWHT 600 °C	2.32 ± 0.44
BM PWHT 700 °C	1.80 ± 0.16
BM PWHT 800 °C	1.58 ± 0.20

Table 3 - Electrochemical parameters in solution containing NaCl concentration 19% wt.

Sample	E _{corr} (mV) (Ag/AgCl)	I _{pass} (μA/cm ²)	E _{pit} (mV) (Ag/AgCl)	E _{prot} (mV) (Ag/AgCl)
BM No PWHT	-243.5 ± 28.5	0.79 ± 0.08	127.0 ± 23.1	-24.2 ± 20.0
BM PWHT 600 °C	-267.5 ± 5.0	0.84 ± 0.02	199.3 ± 33.8	-12.5 ± 5.0
BM PWHT 700 °C	-246.2 ± 14.0	0.86 ± 0.08	197.0 ± 19.8	-53.0 ± 9.9
BM PWHT 800 °C	-232.2 ± 22.2	0.77 ± 0.08	131.0 ± 16.5	-33.0 ± 19.7
WJ No PWHT	-211.0 ± 1.0	9.92 ± 6.2	-43.0 ± 15.1	29.6 ± 23.5
WJ PWHT 600 °C	-217.5 ± 21.9	3.00 ± 1.26	-49.5 ± 0.7	8.9 ± 0.4
WJ PWHT 700 °C	-197.0 ± 9.0	1.82 ± 0.80	-18.3 ± 9.6	-42.5 ± 25.9
WJ PWHT 800 °C	-217.0 ± 30.0	0.63 ± 0.23	43.0 ± 11.7	-112.9 ± 32.0

Figures

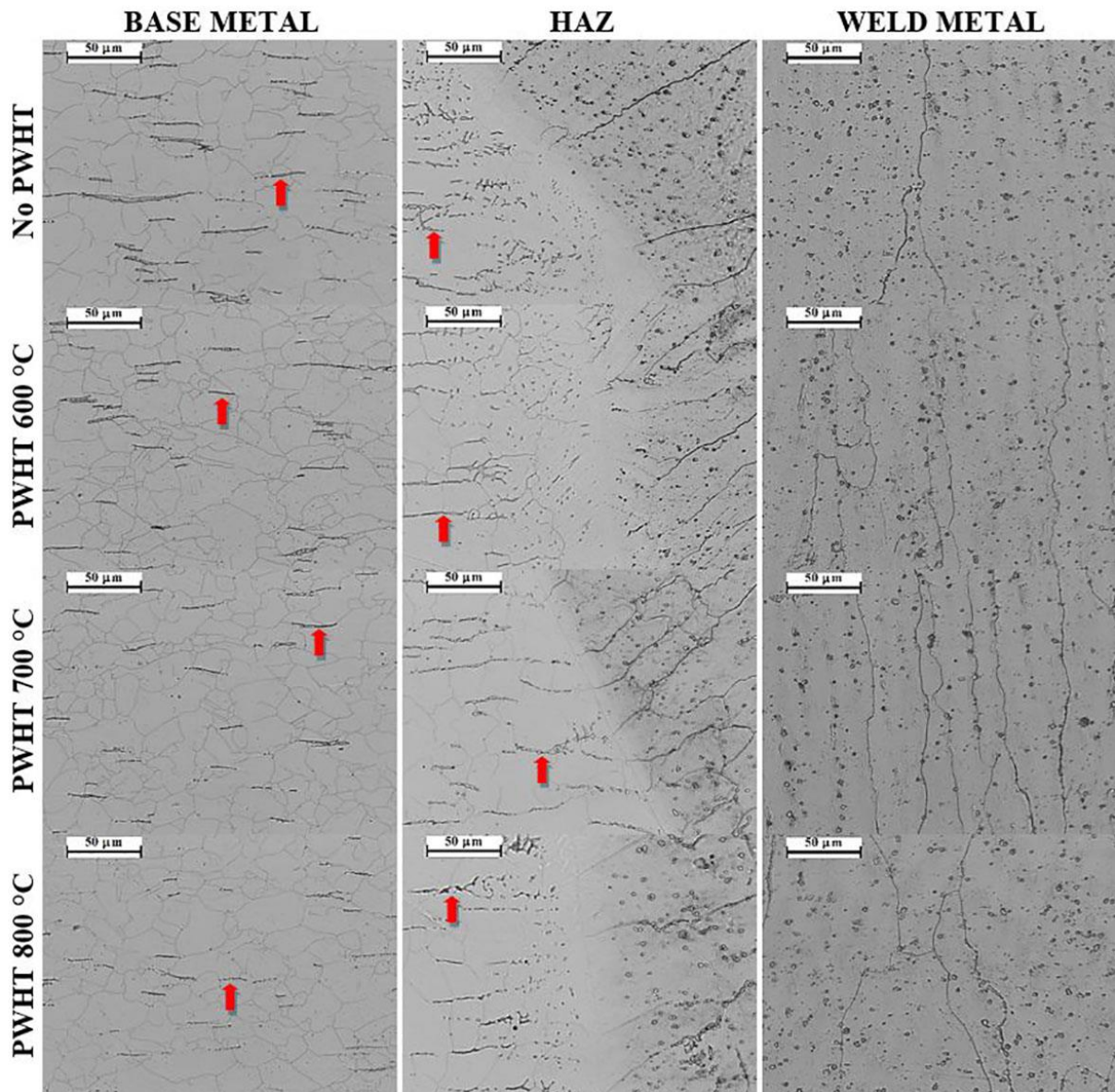


Figure 1. Micrographs of base metal, weld metal, and weld joint before and after PWHT. The arrows points to delta ferrite.

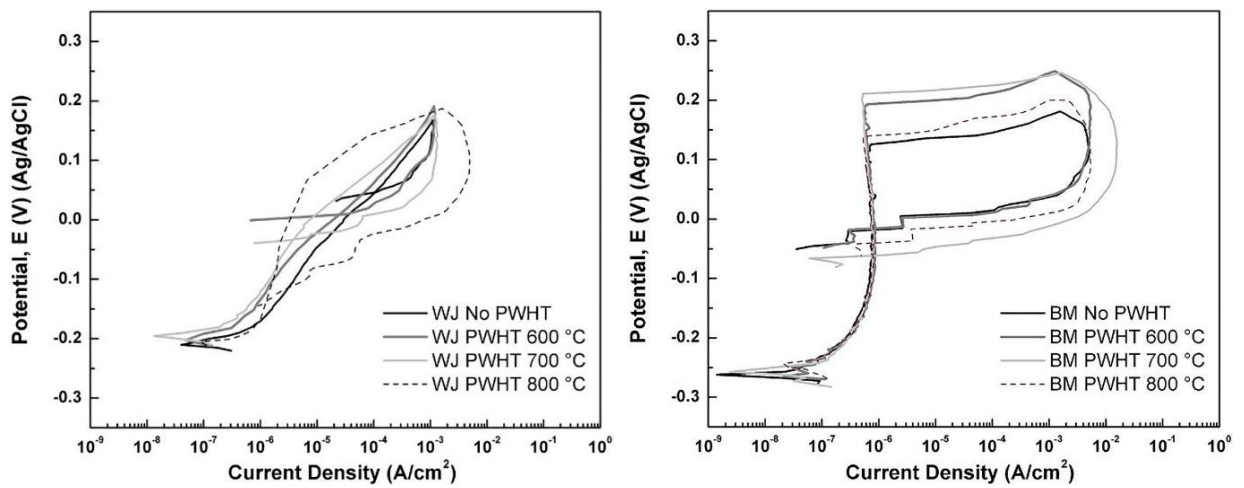


Figure 2 - Polarization curves for base metal (right) and weld joints (left) as welded and after PWHT in 19% wt. NaCl solution.

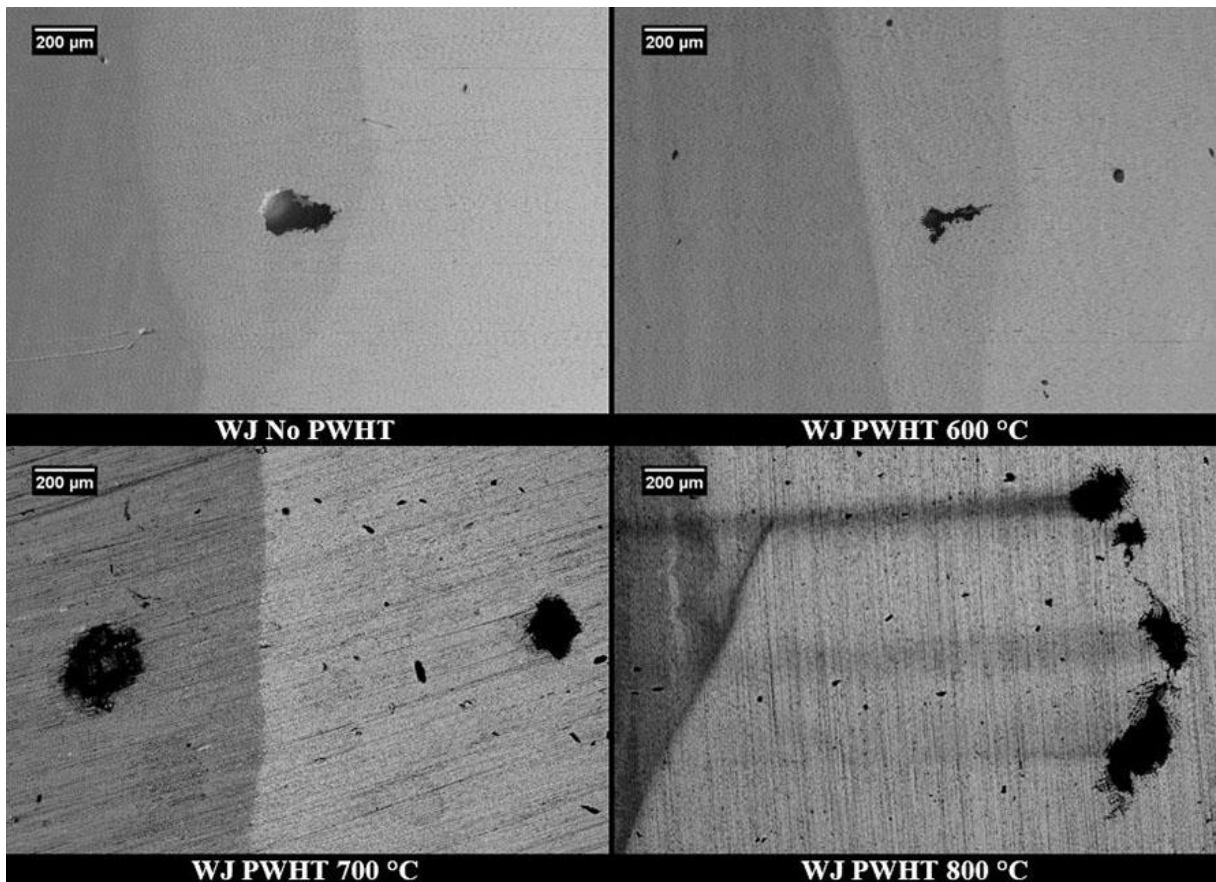


Figure 3 - SEM micrographs of weld joints as welded and after PWHT after cyclic polarization.

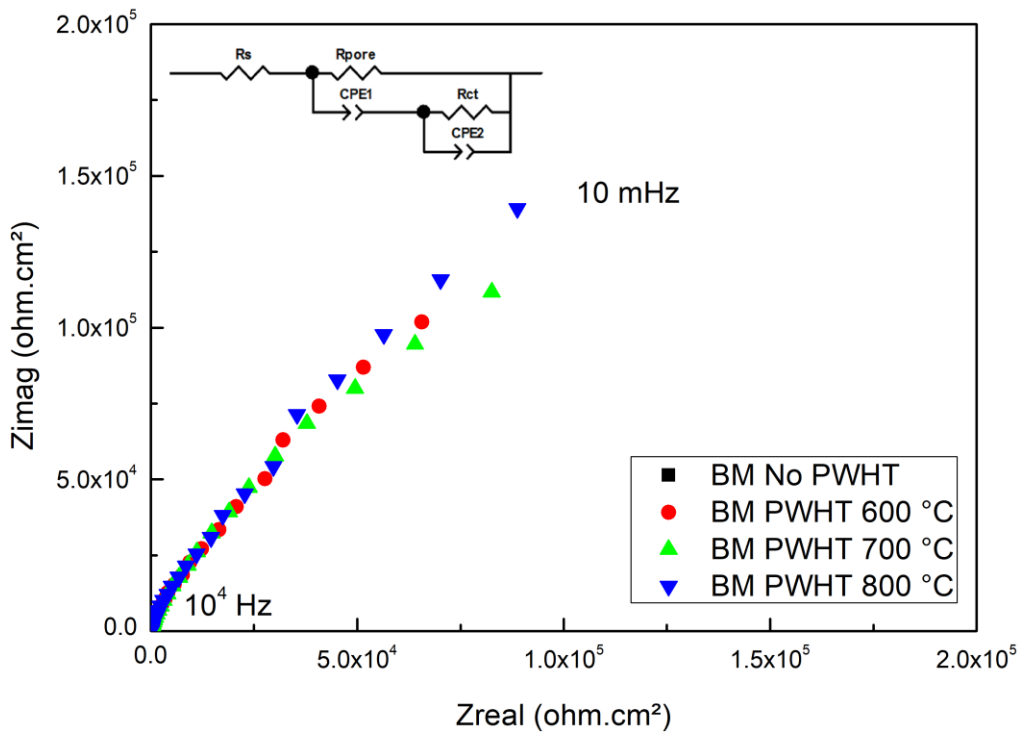


Figure 4 – Nyquist diagrams for base metal as welded and after PWHT in pH 4.0 containing 19% wt. NaCl solution.

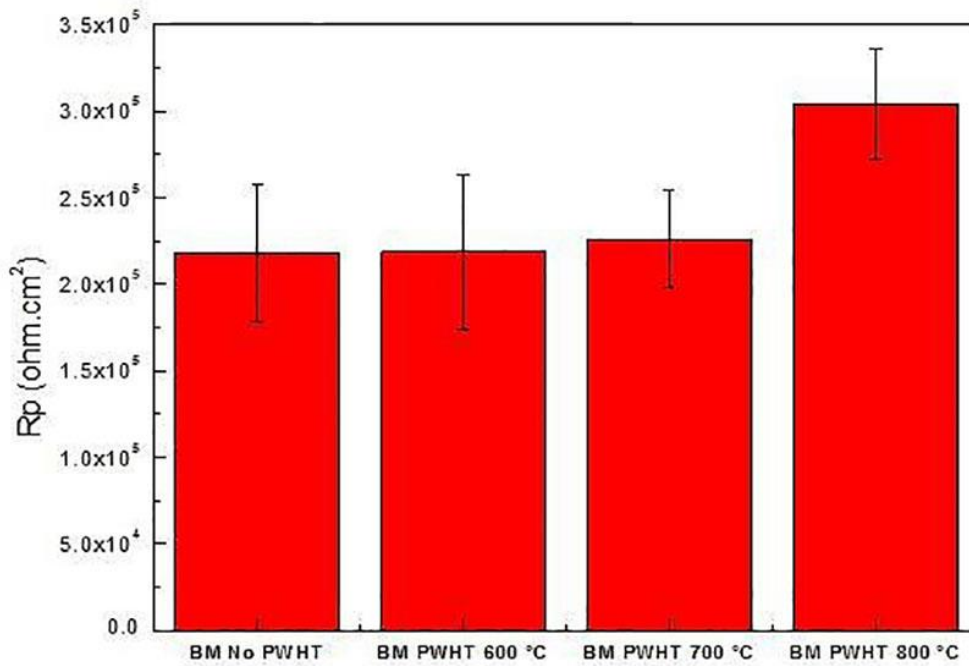


Figure 5 - Average of R_p between the measurements in base metal before and after PWHT in 19% wt. NaCl solution pH 4.0.